Vacuum 109 (2014) 385–396

Contents lists available at ScienceDirect

Vacuum

journal homepage: www.elsevier.com/locate/vacuum

Time-dependent rarefied gas flow of single gases and binary gas mixtures into vacuum

Manuel Vargas [a], Steryios Naris [a, *], Dimitris Valougeorgis [a], Sarantis Pantazis [b], Karl Jousten [b]

[a] Department of Mechanical Engineering, University of Thessaly, 38334 Volos, Greece
[b] Physikalisch-Technische Bundesanstalt (PTB), Abbestr. 2-12, 10587 Berlin, Germany

ARTICLE INFO

Article history:
Received 31 March 2014
Received in revised form
13 June 2014
Accepted 20 June 2014
Available online 1 July 2014

Keywords:
Unsteady vacuum gas dynamics
Binary mixtures
Gas separation
DSMC
Hybrid models
Rarefied gas dynamics

ABSTRACT

Time-dependent flows of single gases and binary gas mixtures with various molar fractions from a chamber through a short tube into vacuum are examined by simulations and experiments. The main goal is the comparison of the flow behaviour between pure gases and binary mixtures including the investigation of the gas separation effect. The simulations are based on an explicit hybrid scheme, coupling at each time step the tube flow rate estimated from a database accordingly constructed via a DSMC solver to the gas pressure in the chamber obtained by a mass conservation equation. Computational results describing the expansion process in terms of the temporal evolution of pressure in the chamber as well as of the total and species flow rates through the tube are reported. Comparison between computational and the corresponding deduced experimental pressures deduces a difference of about 10% which may be explained by accumulation of uncertainties in the time sequence. The binary gas mixture pressure evolution curves are always bounded by the corresponding ones of the components of the mixture flowing as single gases and the tube conductance varies in the opposite direction to that of the weighted mean of the component molar masses. Gas separation is monotonically increased as we move from the viscous towards the free molecular regime, while the rate with which gas separation is increased has a maximum in the transition regime. The equivalent single gas approach provides a reasonable estimate provided that the molar fraction of the light gas and the ratio of heavy to light molar mass are not too high.

1. Introduction

Industrial applications under various vacuum conditions, where the involved gas transport changes with time, include coating processes involving load locks like CD/DVD metallization or bottle coating, drying processes, leak detection, processes in MEMS, etc. Despite their frequent occurrence, time-dependent rarefied gas flows have attracted limited attention, both computationally and experimentally. This is attributed to the increased computational effort (the time dimension is added) and to the more demanding and expensive experimental work (rapid changes of pressure and temperature in time).

Recently, there has been some effort in simulating time-dependent rarefied gas flows through capillaries of circular cross-section. Based on the linearized Bhatnagar–Gross–Krook kinetic model equation, the unsteady fully developed flow in long tubes has been modelled [1], while the Direct Simulation Monte Carlo (DSMC) method has been applied to simulate the transient flow of a rarefied gas through an orifice [2] and a short tube [3]. In all cases, the upstream and downstream boundary conditions remain constant with respect to time and therefore the time needed to reach steady-state conditions is in the order of microseconds (μs). These prototype flow configurations are mainly of theoretical interest, since in typical fast industrial vacuum processes the characteristic times are in the millisecond or second range.

The Physikalisch–Technische Bundesanstalt (PTB) has developed a calibration facility, where the response and relaxation times of vacuum gauges due to rapid pressure changes can be measured [4,5]. This is realized by gas expansion from a high pressure upstream vessel to a low pressure downstream vessel via an exchangeable duct and a very fast opening valve. The time scale of

* Corresponding author.
E-mail address: snaris@mie.uth.gr (S. Naris).

http://dx.doi.org/10.1016/j.vacuum.2014.06.024
0042-207X/

these expansions is similar to fast industrial applications. In this study we investigate how flows of single gas species compare with binary mixtures in such gas expansions.

Simulating this flow configuration solely on kinetic principles is computationally impractical due to the size of the computational domain, which must include the whole volume of the two chambers, in connection with the required very small time step. By taking advantage of the specific characteristics of the flow to introduce acceptable simplifications in modelling, we may greatly reduce the computational effort.

A general approach has been introduced to model the time-dependent flow through a long tube connecting the two chambers [6]. The results include the tube pressure variation in time and space as well as the pressure variation in the two chambers and are valid in the whole range of the Knudsen number. However, this approach is limited to flow configurations where the capillary is very long and the volumes of the capillary and the chambers as well as the corresponding characteristic times are of the same order.

The evolution of the flow through short tubes connecting two chambers has been recently modelled in a hybrid manner [7]. At each time step, based on kinetic theory, a steady-state flow configuration is solved to estimate the amount of gas passing through the tube (micro model) and then the pressure in the two vessels is updated by applying the mass conservation principle and the equation of state (macro model). It is noted that the steady-state kinetic flow rates at each time step are obtained from an adequately dense kinetic database which has been pre-constructed for this purpose and whenever needed interpolation is performed. Based on this approach, the variation of the pressure in the chambers and of the flow rate through the tube with respect to time is provided for several configurations. The theoretical background and a detailed description on the advantages of such hybrid type simulations are given in Ref. [8], where several multi-scale methodologies are analysed. Similar methodologies exploiting time scale separation in a simple manner have also been implemented before in unsteady molecular flows related to filling, exhaust and pumpdown times in pipes and vacuum systems [9] as well as in micro-actuators modelling [10,11].

In the present work, the hybrid modelling approach introduced in Ref. [7] is implemented to computationally investigate the time-dependent flow of various single gases and binary gas mixtures from an upstream vessel through a very short tube into high vacuum. The flow characteristics of pure gases and binary mixtures are compared and the effect of gas separation is analysed. The investigation is accompanied with corresponding experimental work performed at the modified PTB dynamic gas expansion facility [4,5]. The detailed flow configuration and parameters are given in Section 2. Then, the modelling procedure, with the involved micro and macro models are presented in Section 3, while the experimental set-up with the associated measurement procedure are described in Section 4. The obtained results are presented and discussed in Section 5. Finally, in Section 6 some concluding remarks are provided. The Appendix includes the computational data related to the micro model.

2. Flow configuration and parameters

The system under consideration is shown in Fig. 1 and consists of two chambers denoted by A and B, which are connected by a short tube of length L and radius R. The two containers have large but finite volumes V_A and V_B, with $V_A \ll V_B$, while the volume of the capillary V_C is negligibly small compared to the volume of the chambers ($V_C \ll V_A$).

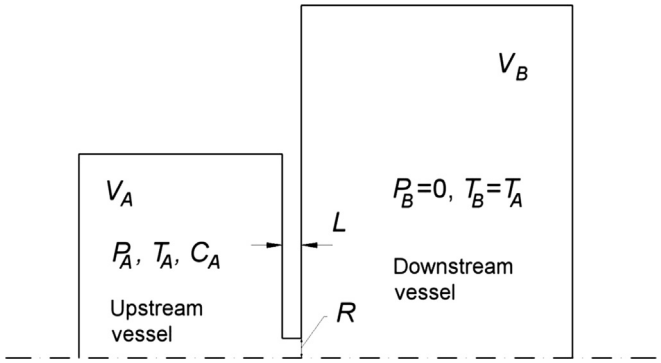

Fig. 1. View of the investigated set-up with geometrical and flow parameters.

In chamber A, at time $t = 0$, the state of a single gas is defined by its initial pressure $P_A^{(0)}$ and temperature $T_A^{(0)}$, connected by the equation of state written as

$$P_A^{(0)} V_A = N_A^{(0)} R^* T_A^{(0)}, \tag{1}$$

where $N_A^{(0)}$ is the initial number of moles in container A and $R^* = 8.314$ J/mol/K is the global gas constant. In the case of a binary gas mixture its initial state is defined by the initial pressure and temperature plus the molar fraction given by Ref. [12]

$$C_A^{(0)} = \frac{N_{1A}^{(0)}}{N_{1A}^{(0)} + N_{2A}^{(0)}} = \frac{P_{1A}^{(0)}}{P_{1A}^{(0)} + P_{2A}^{(0)}}. \tag{2}$$

Here, $N_{iA}^{(0)}$ and $P_{iA}^{(0)}$, with $i = 1, 2$, are the initial number of moles and partial pressure respectively of the each component in container A, while the initial total number of moles is given by $N_A^{(0)} = N_{1A}^{(0)} + N_{2A}^{(0)}$ and similarly the initial total pressure is $P_A^{(0)} = P_{1A}^{(0)} + P_{2A}^{(0)}$. The molar masses of the two species are m_1 and m_2 ($m_1 < m_2$), while the initial molar mass of the mixture is defined as [12]

$$m_A^{(0)} = C_A^{(0)} m_1 + \left(1 - C_A^{(0)}\right) m_2. \tag{3}$$

Therefore, $C_A^{(0)}$ actually refers to the molar fraction of the light species and for $C_A^{(0)} = 1$ and 0 the corresponding states of the single light and heavy gas respectively are recovered.

Furthermore, initially the gas rarefaction in chamber A is characterized by the initial Knudsen number defined as

$$Kn_A^{(0)} = \frac{\sqrt{\pi}}{2} \frac{\mu_A^{(0)} \upsilon_A^{(0)}}{P_A^{(0)} R} \tag{4}$$

where $\upsilon_A^{(0)} = \sqrt{2R^* T_A^{(0)} / m_A^{(0)}}$ is the initial molecular velocity of the gas and $\mu_A^{(0)}$ is the gas viscosity at temperature $T_A^{(0)}$ and molar fraction $C_A^{(0)}$. In the case of a single gas, $\upsilon_A^{(0)}$ corresponds to the most probable velocity. In chamber B, the pressure is taken equal to zero.

Then, the valve at the inlet of the tube rapidly opens and the time-dependent gas expansion between the two vessels evolves. In the downstream vessel B we assume $P_B = 0$ all the time, since its volume is much larger than the volume of vessel A and the vacuum pump is connected to vessel B. The molar flow rate denoted by $\dot{N}(t)$ gradually decreases, as the pressure difference between the two vessels is reduced asymptotically tending to zero.

Table 1
Geometrical and flow parameters.

Data	Notation	Value
Volume of upstream vessel	V_A	3.1 L
Volume of downstream vessel	V_B	185 L
Tube length	L	0.4962 ± 0.01 mm
Tube diameter	$D = 2R$	1.0113 ± 0.005 mm
Volume of tube	V_C	0.39×10^{-6} L
Initial upstream pressure	$P_A^{(0)}$	1000 Pa
Temperature	$T_A^{(0)}$	295 K
Downstream pressure	P_B	0 Pa

The objective is to compute the time evolution of the upstream pressure $P_A(t)$ and the molar flow rate $\dot{N}(t)$ through the tube for time $t > 0$. In the expansion of a binary gas mixture, in addition to the above quantities, the time evolution of the molar fraction of the mixture $C_A(t)$, is deduced. In this latter case, at time t the molar flow rate is the summation of the molar flow rates of the two species, i.e. $\dot{N}(t) = \dot{N}_1(t) + \dot{N}_2(t)$, while the upstream pressure of the mixture may be written as $P_A(t) = P_{1A}(t) + P_{2A}(t)$, where $P_{1A}(t)$ and $P_{2A}(t)$ are the partial pressure of each species in the container. The computational solution yields the molar flow rates and the partial pressures of the species as well. Experimentally, the objective is to measure for both single gases and mixtures the upstream pressure $P_A(t)$ in terms of time. In the present work we base our analysis on the molar flow rates instead of the mass flow rates mainly due to the fact that the molar mass of the mixture depends on the molar fraction and therefore will vary with time.

The specific geometrical data of the two vessels and the connecting tube along with the initial conditions in vessel A are given in Table 1. The condition $V_C \ll V_A \ll V_B$, which is important for the implementation of the hybrid scheme presented in Section 3, is fulfilled. The aspect ratio L/D of the tube is about 0.5. The initial gas pressure and temperature are always set to the specific values, while the pressure ratio of the downstream over the upstream vessel pressure throughout the expansion process is zero. Thus, the proper estimation of the molar flow rate $\dot{N}(t)$ requires a nonlinear treatment and inclusion of end effects.

The present computational and experimental investigation of the above prescribed time-dependent flow configuration is performed for the single monatomic gases of He, Ne, Ar and Kr, and for the binary gas mixtures of He–Ne, He–Ar and He–Kr, with $C_A^{(0)} \in [0, 1]$. In Table 2 the molar masses, the molecular diameters, the viscosities and the most probable velocities along with the associated initial Knudsen numbers for $R = 0.5$ mm are tabulated. The species diameters and viscosities have been obtained from Eq. (4.62) and Table A1 in Ref. [13] respectively, with the latter ones converted from 273 K to 295 K assuming hard sphere (HS) molecules. The data in the last two columns of Table 2 related to the characteristic times are discussed in the next section. Initially, the gas state is in the slip regime and then as the expansion evolves it will be in the transition and finally in the free molecular regime. This holds also in the expansion of the binary gas mixtures, the properties of which may be readily defined from the data in Table 2, provided that the molar fraction of the mixture is specified. Depending on the specific value of the molar fraction, the properties of the binary gas mixtures will be somewhere in the range of the corresponding values of its components.

The molar mass ratio m_2/m_1 of He–Ne, He–Ar and He–Kr, is about 5, 10 and 21 respectively. This range of m_2/m_1 is large enough to investigate the effect of the molar mass ratio on the flow properties of the binary gas. Similarly the initial molar fraction $C_A^{(0)}$ is varied. The dependency of the results on these two quantities provides some insight in the separation phenomena, which is present in binary gas flows, as well as in the identification of differences (and similarities) between single gases and binary gas mixtures.

3. Computational approach

In principle, the gas expansion configuration described in Section 2, may be modelled by applying a suitable kinetic methodology over the entire flow domain. The simulation domain however, is very large both in time and space, making this approach computationally impractical. Thus, in a recent work [7], the expansion process of a single gas from a large container through a small tube has been modelled by a simple explicit-type hybrid approach. The mass flow rate of the gas passing through the tube at time t is obtained by a micro model, which is based on a suitable kinetic solver, and then the evolution of the macroscopic quantities in the chamber at time $t + \Delta t$, where Δt is the macroscopic time step, is predicted by a macro model, where mass conservation is applied.

This hybrid approach, extended in a straightforward manner to include the case of binary gas mixture expansion, is implemented in the present work. The macro model is applied to the upstream chamber and the micro model to the tube. The corresponding macro and micro characteristic times are defined as [7]

$$t_M = \frac{V_A/R^2}{\upsilon_A^{(0)}} \quad \text{and} \quad t_m = \frac{R}{\upsilon_A^{(0)}} \tag{5}$$

respectively and based on the specific geometrical data and physical properties of the gases they are computed and provided in Table 2. It is seen that $t_m \ll t_M$. These observations imply that the region and the period over which the macroscopic quantities may vary are significantly larger in the chamber than in the tube and it is reasonable to exploit the space and time scale separation implementing the hybrid scheme [7,8]. Here, the formulation is provided for the more general case of the binary gas mixture, while the corresponding simplified expressions for the single gas expansion are readily deduced by setting the molar fraction equal to zero or one.

Table 2
Physical parameters, initial Knudsen numbers and characteristic times for He, Ne, Ar and Kr.

Gas	Molar mass m (g/mol)	Molecular diameter $d \times 10^{10}$ (m)	Viscosity at 295 K $\mu \times 10^5$ (Pa s)	Most probable molecular velocity at 295 K υ_0 (m/s)	Initial Knudsen at 1000 Pa and 295 K for $R = 0.5$ mm $Kn_A^{(0)}$	Characteristic kinetic time t_m (μs)	Characteristic macroscopic time t_M (s)
He	4.002	2.175	1.939	1107.0	3.803E-02	0.452	11.20
Ne	20.18	2.580	3.093	493.0	2.703E-02	1.014	25.15
Ar	39.95	3.628	2.201	350.4	1.367E-02	1.427	35.39
Kr	83.80	4.164	2.420	241.9	1.038E-02	2.067	51.26

Starting with the macro model, the gas properties in chamber A, at time t, are interrelated by the equation of state for each species, written as

$$P_{i,A}(t)V_A = N_{i,A}(t)R^*T_A, \quad i = 1,2 \tag{6}$$

where $P_{i,A}(t)$ and $N_{i,A}(t)$, with $i = 1, 2$ are the partial pressures and the number of moles of each species and T_A is the temperature of the mixture, which is assumed to remain constant through the entire process. This is a reasonable approximation since the gas expansion is not very rapid and it has also been confirmed by measurements for the specific geometry and parameters of Table 1. In addition, the pressure in the container at each time step is taken to be uniform. The temporal evolution of the number of moles of each species in the chamber is defined by the ordinary differential equations

$$\frac{dN_{i,A}}{dt} = -\dot{N}_i(t), \quad i = 1,2 \tag{7}$$

where $\dot{N}_i(t)$ is the molar flow rate of species i, leaving in a unit of time the upstream container and are computed at each time step by the micro model. Eqs. (6) are differentiated with respect to time and then they are combined with Eqs. (7) to yield the pressure evolution equations

$$\frac{dP_{i,A}}{dt} = -\dot{N}_i(t)\frac{R^*T_A}{V_A}, \quad i = 1,2 \tag{8}$$

with initial conditions

$$P_{1,A}(0) = P_{1,A}^{(0)} = C_A^{(0)}P_A^{(0)}, \quad P_{2,A}(0) = P_{2,A}^{(0)} = \left(1 - C_A^{(0)}\right)P_A^{(0)} \tag{9}$$

It is noted that the ordinary differential Eqs. (8) are nonlinear since the molar flow rates $\dot{N}_i(t)$ depend on the chamber pressures $P_{i,A}$. They are solved numerically and once the partial pressures are estimated, the number of moles $N_{i,A}(t)$ is obtained by Eqs. (6) and the molar fraction of the mixture $C_A(t)$ is readily deduced as

$$C_A(t) = \frac{N_{1A}(t)}{N_{1A}(t) + N_{2A}(t)}. \tag{10}$$

The initial value of the molar fraction is $C_A(0) = C_A^{(0)}$. The evolution of the total pressure $P_A(t)$ and number of moles $N_A(t)$ are computed by summing the corresponding quantities of each species. Similarly, the Knudsen number in chamber A varies with time and it is defined as

$$Kn_A(t) = \frac{\sqrt{\pi}}{2}\frac{\mu_A(t)\upsilon_A(t)}{P_A(t)R} \tag{11}$$

where $\mu_A(t)$ and $\upsilon_A(t) = \sqrt{2R^*T_A/m_A}$ are the viscosity and characteristic molecular velocity respectively, which both depend on the molar fraction $C_A(t)$. As it has been noted, the molar mass of the mixture in the chamber A varies with time according to

$$m_A(t) = C_A(t)m_1 + (1 - C_A(t))m_2. \tag{12}$$

Turning now to the micro model, the molar flow rates $\dot{N}_i(t)$, $i = 1, 2$ are estimated at each time step based on a database which has been accordingly prepared by a DSMC solver [13,14]. At time t, based on the current upstream conditions, the pressure driven rarefied gas flow through a tube of $L = R = 0.5$ mm ($L/R = 1$) into vacuum ($P_B/P_A = 0$) is simulated. The flow is also characterized by the upstream Knudsen number Kn_A, which varies with time. This flow configuration in the case of single gas flow has been extensively investigated and results are available in a wide range of the reference Knudsen number via deterministic [15–18] and stochastic [19–23] kinetic solvers. The corresponding binary gas flow has received much less attention [24], mainly due to the significantly increased computational effort. The flow is specified by the above parameters plus the definition of the type of gas mixture as well as its molar fraction C_A, which like the Knudsen number varies with time.

For the needs of the present work, a dense kinetic database of steady-state flow rates has been constructed for the mixtures of He–Ne, He–Ar and He–Kr in a wide range of $Kn_A \in [10^{-2}, \infty]$ and for various $C_A \in [0, 1]$ assuming HS molecules and purely diffuse wall reflection (see Table 3 of the Appendix). The DSMC simulations have been performed by using the Simplified Bernoulli Trials (SBT) scheme [14] for the particle collisions in order to reduce the computational resources (memory). The numerical uncertainty of the flow rates is less than 1%. Computational details of the DSMC solution are presented in the Appendix. Then, at each time step, the dimensionless flow rates of each species J_1, J_2 and the total flow rate $J = J_1 + J_2$, are obtained by accordingly interpolating between the data of Table 3 and they are related to the molar flow rate according to

$$\dot{N}_i(t) = \frac{N_A(t)}{V_A}\pi R^2 \upsilon_A(t) J_i(t), \quad i = 1,2. \tag{13}$$

Since the computed flow rates of the three binary gas mixtures have not been reported before in the literature in such a wide range of parameters and since they are also important in the solution of Eqs. (8), they are provided in tabulated form in the Appendix (see Table 3). These data can also be used for reference purposes in future computational and experimental works.

A dimensional quantity, which is of major importance in industrial applications, is the unsteady conductance of each component through the tube, which is defined as

$$Q_i(t) = \frac{\dot{N}_i R^*T_A}{P_A(t)} = J_i(t)\pi R^2 \upsilon_A(t), \quad i = 1,2 \tag{14}$$

while the total conductance is $Q(t) = Q_1(t) + Q_2(t)$.

Based on the above formulation, the procedure to advance from time t to $t + \Delta t$ is as follows:

1. At time t the quantities $P_{i,A}(t)$, $N_{i,A}(t)$, with $i = 1, 2$, $C_A(t)$ and $Kn_A(t)$ are known from the previous time step.
2. Based on the input parameters $Kn_A(t)$ and $C_A(t)$, the flow rates through the tube $J_1(t)$ and $J_2(t)$ for the specific gas mixture are computed by interpolating between the steady-state DSMC results in Table 3. The molar flow rates $\dot{N}_i(t)$, $i = 1, 2$ are estimated from Eq. (13).
3. Then, Eqs. (8) are numerically integrated in time to yield the gas pressures $P_{i,A}(t + \Delta t)$, $i = 1, 2$.
4. The code returns to Step 1 and computes the remaining chamber parameters, namely the number of moles $N_{i,A}(t + \Delta t)$, $i = 1, 2$ of each species, the molar fraction $C_A(t + \Delta t)$ and the Knudsen number $Kn_A(t + \Delta t)$ by Eqs. (6), (10) and (11) respectively.

The marching scheme in time is continued until the equilibrium state is reached.

Results will be described in Section 5. In general, the hybrid model is valid in flows with smooth variations in the upstream pressure, where the main assumptions of isothermal expansion and uniform pressure evolution in chamber A hold. Otherwise, more advanced and much more computationally demanding hybrid schemes must be involved [25].

It is noted here that the values of the geometrical size of the tube and the upstream volume realized in the experiment may be different from the values used for the simulation due to the measurement uncertainties of the geometrical dimensions (see Table 1). This means that there may be a deviation between simulated and real flow rate through the tube and, as a consequence, there is also a deviation in pressure which accumulates over time. This can be easily seen by modelling the pressure evolution assuming a constant conductance Q which results in an exponential decay of the pressure $P_A(t)$ in the upstream vessel of volume V_A:

$$P_A(t) = P_A(0)\exp\left(-\frac{Q}{V_A}t\right) \tag{15}$$

Eq. (15) is applied in Section 5.1 to explain the observed differences between simulations and measurements.

4. Experimental approach

The dynamic pressure standard of the Physikalisch–Technische Bundesanstalt (PTB) has been modified to perform experiments for this investigation. The larger volume V_B (185 L) was kept, but the smaller volume V_A was increased to 3.1 L to reduce the time constant of pressure reduction during the expansion.

The conductance element between the two vessels is a cylindrical tube with the dimensions given in Table 1. Fig. 2 shows the assembled system, with several components denoted. The upstream volume V_A consists of the 3.0 L volume (A) and a smaller 0.1 L volume, on which the pressure measurement devices (B) are attached. The dosing valve (C), through which the gas is introduced to the system, is also connected to the same volume. The expansion starts when the fast opening valve (D) is activated, with the full conductance obtained within 4.6 ms [5]. The test gas or mixture of gases is released from the small volume through an orifice and the opened valve to the large volume (E). The turbomolecular pump attached to V_B is operating all the time during the expansion to maintain high vacuum behind the orifice. Either volume may be evacuated or filled independently with a test gas or mixture up to a desired pressure of less than 100 kPa.

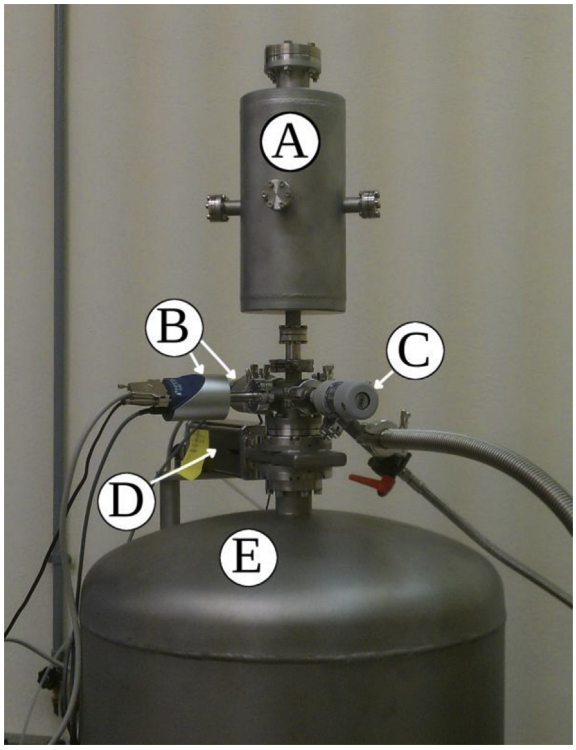

Fig. 2. View of the experimental apparatus used in Ref. [4], where (A) is the additional 3.0 L upstream volume, (B) are the capacitance diaphragm gauges, (C) is the dosing valve, (D) is the fast opening valve and (E) is the large downstream volume.

The pressure has been measured at the upstream volume by Capacitance Diaphragm Gauges (CDGs) by Inficon®, custom-manufactured to provide data with an update time of 0.7 ms. Previous studies [4] have shown that they are able to follow pressure changes even for the fastest expansion of our system. The values of their additional volumes have been taken into account in the computations. Furthermore, the temperature has been measured by a thermocouple connected to a nanovoltmeter. It has been found that the temperature drop was much less than 1 K, thus leading to the conclusion that the flow is isothermal. The uncertainty budget for pressure measurement has been presented in Ref. [26] for nitrogen flow. It was found that a maximum of 2.5% expanded uncertainty ($k = 2$) may be expected for fast flows (less than 1 s in duration). Further details about the experimental facility may be found in Refs. [4,26].

As an extension of previous work with pure gases, the flow of binary gas mixtures was investigated. The mixture uniformity was ensured by examining different homogenization methods. Two fans were placed inside the 3.1 L volume. They were oriented at different heights and opposite directions towards the walls, not facing the vessel ports. The additional volume of the fans has been taken into account in the calculations. The relatively large vessel volume and adjustable dosing valve allow the accurate insertion of a specific amount of gas, leading to good reproducibility of the measurement. An expansion of He–Kr 50%–50% mixture has been examined as a test case. An expansion is performed without activating the fans and the measurement has been repeated after additionally homogenizing the mixture with the fans for 0.5 h. Small differences between the two measurements were within measurement uncertainties, leading to the conclusion that the mixture has been sufficiently homogeneous even without activating the fans.

Based on the above the pressure temporal evolution has been measured for all single gases and binary mixtures under consideration and the experimental data are reported in the next section.

5. Results and discussion

Computational and experimental results are presented for the single gases of He, Ne, Ar and Kr as well as for the binary gas mixtures of He–Ne, He–Ar and He–Kr with $C_A^{(0)} \in [0,1]$. The values $C_A^{(0)} = 0$ and $C_A^{(0)} = 1$ correspond to single gas flows of the heavy and light species of the mixture respectively. In Section 5.1 the computed and measured evolutions of the gas pressure $P_A(t)$ in the upstream chamber are reported and a comparison between corresponding results is performed. This comparison includes single gases and binary gas mixtures. In Sections 5.2 and 5.3 only computational results are presented. The time variation of the dimensionless flow rates $J(t)$, molar flow rates $\dot{N}(t)$ and conductance $Q(t)$ of all three mixtures and of their components are provided in Section 5.2. In the same section the gas separation phenomena is analysed by investigating the evolution of the ratio $J_1(t)/J_2(t)$. In Section 5.3 the validity and range of applicability of the so-called “equivalent single gas” approach is examined.

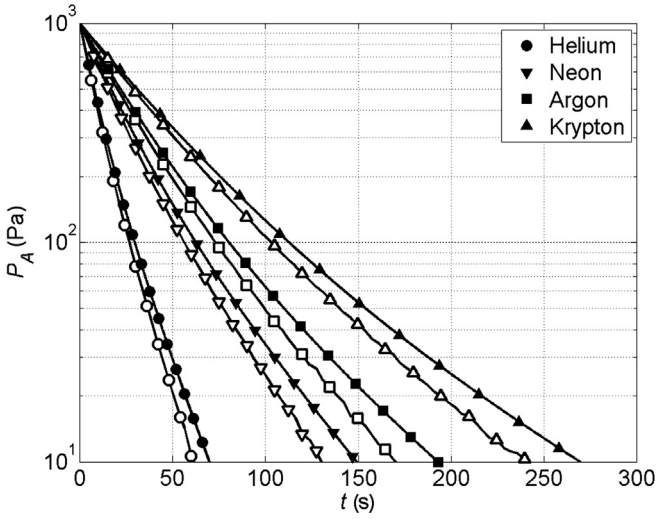

Fig. 3. Temporal evolution of pressure $P_A(t)$ for the single gases of He, Ne, Ar and Kr; computed (filled symbols), measured (empty symbols).

5.1. Computed and measured temporal evolution of chamber pressure

The computed and measured temporal evolution of pressure $P_A(t)$ in the upstream vessel for the single gases of He, Ne, Ar and Kr are plotted in Fig. 3 and for the binary gas mixtures He–Ne, He–Ar and He–Kr, with $C_A^{(0)} = [0.1, 0.5, 0.9]$ in Fig. 4. In all cases at $t = 0$ the initial pressure is $P_A^{(0)} = 1000$ Pa and the upstream pressure $P_A(t)$ has been plotted until it reaches $P_A = 10$ Pa.

In Fig. 3, the required time to reach $P_A = 10$ Pa varies for each gas, from about 60 s for He up to about 275 s for Kr. Similarly, in Fig. 4, as the molar mass of the mixture $m_A^{(0)}$ (see Eq. (3)) is increased (i.e., as the initial molar fraction $C_A^{(0)}$ of the lighter gas species is decreased) the time needed to reach a certain pressure is increased. The binary gas mixture pressure evolution curves are always bounded by the corresponding ones of the two components of the mixture flowing as single gases and more precisely from the light gas curve ($C_A^{(0)} = 1$) from below and the heavy gas curve ($C_A^{(0)} = 0$) from above. In both Figs. 3 and 4 even though the computational and experimental results are qualitatively in agreement, the computational expansion is always slower compared to the corresponding experimental one and therefore as time is increased the differences are also increased. For the time period related to the fast pressure drop from 1000 to 100 Pa the agreement is very good, while from 100 to 10 Pa, where the expansion process becomes slower the discrepancies are gradually increased.

To investigate this issue, both the computational and experimental data reported in Fig. 3 (for single gases), are accordingly reduced in dimensionless form and are presented in Fig. 5 in compact form in terms of the inverse Knudsen number $[Kn_A]^{-1}$, where $Kn_A(t)$ is given by Eq. (11), versus the dimensionless time $\tau = t/t_M$, where t_M is given in Eq. (5). In the vertical axis the variation of $[Kn_A]^{-1}$ corresponds to the pressure drop from 1000 to 10 Pa. This data reduction is straightforward for the computational results, while for the experimental results, is achieved by following in an inverse manner the modelling formulation described in Section 3. The experimental data for all four gases are aligned along a single curve, as shown in Fig. 5, with each gas covering a different range of the inverse Knudsen number, including of course some overlapping. The experimental steady-state flow rate J^{exp} corresponding to this curve is computed and it is found to always be about 10% higher than the corresponding computational flow rate J at each time step.

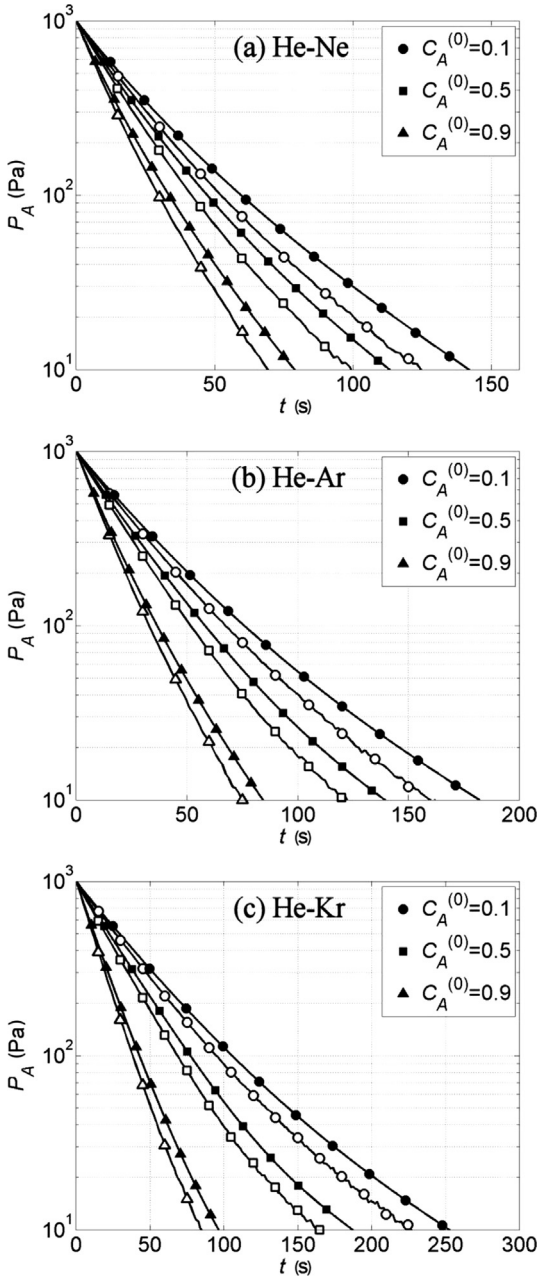

Fig. 4. Temporal evolution of pressure $P_A(t)$ for the binary gas mixtures of (a) He–Ne, (b) He–Ar and (c) He–Kr with various initial molar fractions $C_A^{(0)}$; computed (filled symbols), measured (empty symbols).

As stated before the experimental uncertainties are not more than 2.5%, while the steady-state DSMC results in Table 3 have numerical uncertainties, which do not exceed 1%. It is noted that the single gas flow rates in Table 3 are in excellent agreement with corresponding kinetic and DSMC results previously reported in the literature [18,21,27,28], while good agreement between DSMC and experimental results has been repeatedly observed in the past [20–22,29]. Also, since both pure gases and binary gas mixture computational flow rates show a similar decay compared to the experimental ones the discrepancies are not attributed to binary gas flow peculiarities. Modelling approximations includes the

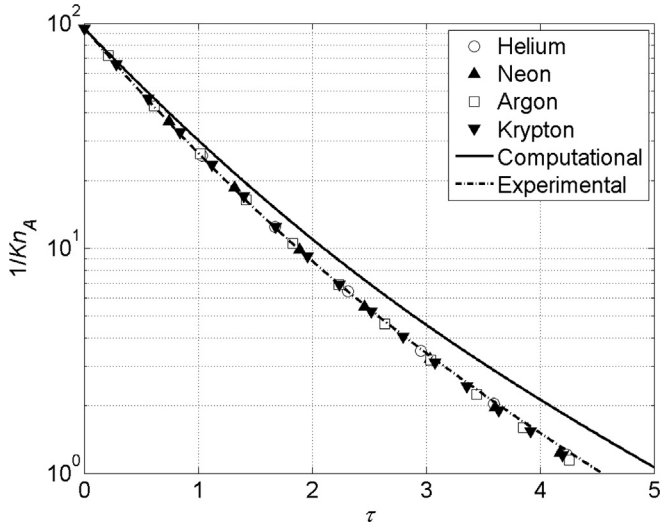

Fig. 5. Experimental results of the gas expansion of He, Ne, Ar and Kr reduced in dimensionless form in a single curve of the inverse Knudsen number $1/Kn_A$ in terms of the dimensionless time τ and comparison with the corresponding computational ones.

intermolecular potential and the gas-surface interaction models. The influence of the former one is small for this type of flows [21,30], while a non-purely diffuse reflection at the walls is not likely the case for most gases applied here. Thus, another explanation for the differences between computed and measured results is the one noted at the end of Section 3, i.e., the geometrical uncertainty of the tube and the volume with its resulting error accumulation for the pressure. For example, based on Eq. (15), an error of 1% in Q or V_A, which can be easily expected from the measurement uncertainties (see Table 1), causes a difference of 5% in the value of pressure obtained by simulations at time equal to 60 s for helium flow. This value has been extracted using $Q = 0.286$ L/s according to the nominal tube dimensions and initial pressure conditions.

5.2. Temporal evolution of flow rates and gas separation analysis

The time variation of the flow rates of the three binary gas mixtures as well as of their components is investigated. Based on these data the separation phenomenon is analysed. All presented results correspond to gas expansion from $P_A^{(0)} = 1000$ Pa down to 1 Pa and therefore the required expansion times are higher than the ones in Section 5.1.

Starting with the total quantities, the temporal evolution of the molar flow rate $\dot{N}(t)$ and of the conductance $Q(t)$ of the binary gas mixtures of He–Ne, He–Ar and He–Kr are given in Fig. 6. These quantities are obtained by adding the corresponding ones of the components of the mixture given by Eqs. (13) and (14) respectively. For each mixture, results are provided for $C_A^{(0)} = [0, 0.1, 0.5, 0.9, 1]$. The case $C_A^{(0)} = 0$ corresponds, depending upon the composition of the gas mixture, to the single gas flow rates of Ne, Ar and Kr, while the case $C_A^{(0)} = 1$ corresponds always to He. Consider the case of He–Ar (Fig. 6b). Both $\dot{N}(t)$ and $Q(t)$ are reduced in time since the pressure difference driving the flow is reduced. As $C_A^{(0)}$ is increased, i.e., as the molar mass $m_A^{(0)}$ becomes smaller, the molar flow rate $\dot{N}(t)$ is reduced faster with time. Also, in the beginning of the process, $\dot{N}(t)$ is higher for higher $C_A^{(0)}$, but after some certain time, which is about the same in all $C_A^{(0)}$, it is the other way around, i.e. it is higher for lower $C_A^{(0)}$. This is related to the associated pressure drop in the chamber, as well as to the fact that the molar fraction of the mixture in the chamber $C_A(t)$ is constantly decreased with time and the molar mass of the mixture $m_A(t)$ given by Eq. (12) is constantly increased, resulting to lower molar flow rates as the expansion process evolves. From the corresponding conductance plots, also shown in Fig. 6b, it is seen that throughout the process the conductance of the mixture for $C_A^{(0)} = [0.1, 0.5, 0.9]$ is between the conductance of pure Ar ($C_A^{(0)} = 0$) from below and of pure He ($C_A^{(0)} = 1$) from above (now is the other way around compared to the pressure evolution). Furthermore, it is observed that the conductance for $C_A^{(0)} = 0$ is actually the same with the one of the binary gas mixture for $C_A^{(0)} = 0.1$, while this is not the case between the conductance for $C_A^{(0)} = 1$ and $C_A^{(0)} = 0.9$. This is a clear indication that gas separation plays a much more important role in the latter than in the former case. Overall, the conductance of the binary gas mixture is monotonically increased as the molar mass of the mixture is reduced. This statement, which applies in single gases, is also valid in the case of gas mixtures in the whole range of gas rarefaction. The above remarks for $\dot{N}(t)$ and $Q(t)$ of He–Ar are qualitatively the same in the cases of the other two mixtures becoming less and more evident for the He–Ne and He–Kr mixtures respectively.

The flow rates J_1, J_2 and the conductance Q_1, Q_2, along with the corresponding total ones are provided for the binary gas mixture of He–Ar with $C_A^{(0)} = [0.1, 0.5, 0.9]$ in Fig. 7. For $C_A^{(0)} = 0.1$, the quantities J_1 and Q_1 of the light species drop much faster than those of the heavy species, while at all times J_2 and Q_2 almost coincide with J and Q respectively. This behaviour is explained, since the light gas, which compared to the heavy one is in a small amount, almost vanishes within a short time period from the upstream vessel. The gas mixture flow characteristics are defined mainly by those of the heavy species throughout the expansion process. In the case of $C_A^{(0)} = 0.5$ initially the flow rates and the conductance of the light and heavy species are very close and decrease slowly. After some time however, J_1 and Q_1 drop rapidly, while J_2 and Q_2 are slightly increased with the total J and Q decreasing very slowly. The difference to the case $C_A^{(0)} = 0.1$ is that now initially the gas mixture flow characteristics are defined by both components, while at a later stage of the expansion process, when the light gas has been significantly reduced in the upstream chamber, the mixture flow is much closer to that of the heavy species. Finally, for $C_A^{(0)} = 0.9$, in the beginning of the expansion process, since J_1 and Q_1 almost coincide with J and Q respectively, the light gas determines the mixture flow characteristics. Then, in a later stage of the process J_1 and Q_1 are reduced, while in parallel J_2 and Q_2, which are initially reduced they start increasing and therefore both components contribute to the total quantities. The resemblance in the qualitative behaviour between J and Q is expected and it has been observed in single gas flows through long channels between corresponding results of the so-called dimensionless flow rate and conductance [31].

In order to investigate the separation phenomena occurring during the time-dependent expansion process, it is useful to study the variation of the ratio $J_1(t)/J_2(t)$, with respect to time. In general, when the flow is in the viscous limit, where there is no separation, the ratio approaches the value

$$\frac{J_1}{J_2} \to \frac{C_A}{1 - C_A}, \tag{16}$$

while in the free molecular limit, where the flow of each mixture component is independent, the ratio becomes

$$\frac{J_1}{J_2} \to \frac{C_A}{1 - C_A}\sqrt{\frac{m_2}{m_1}}. \tag{17}$$

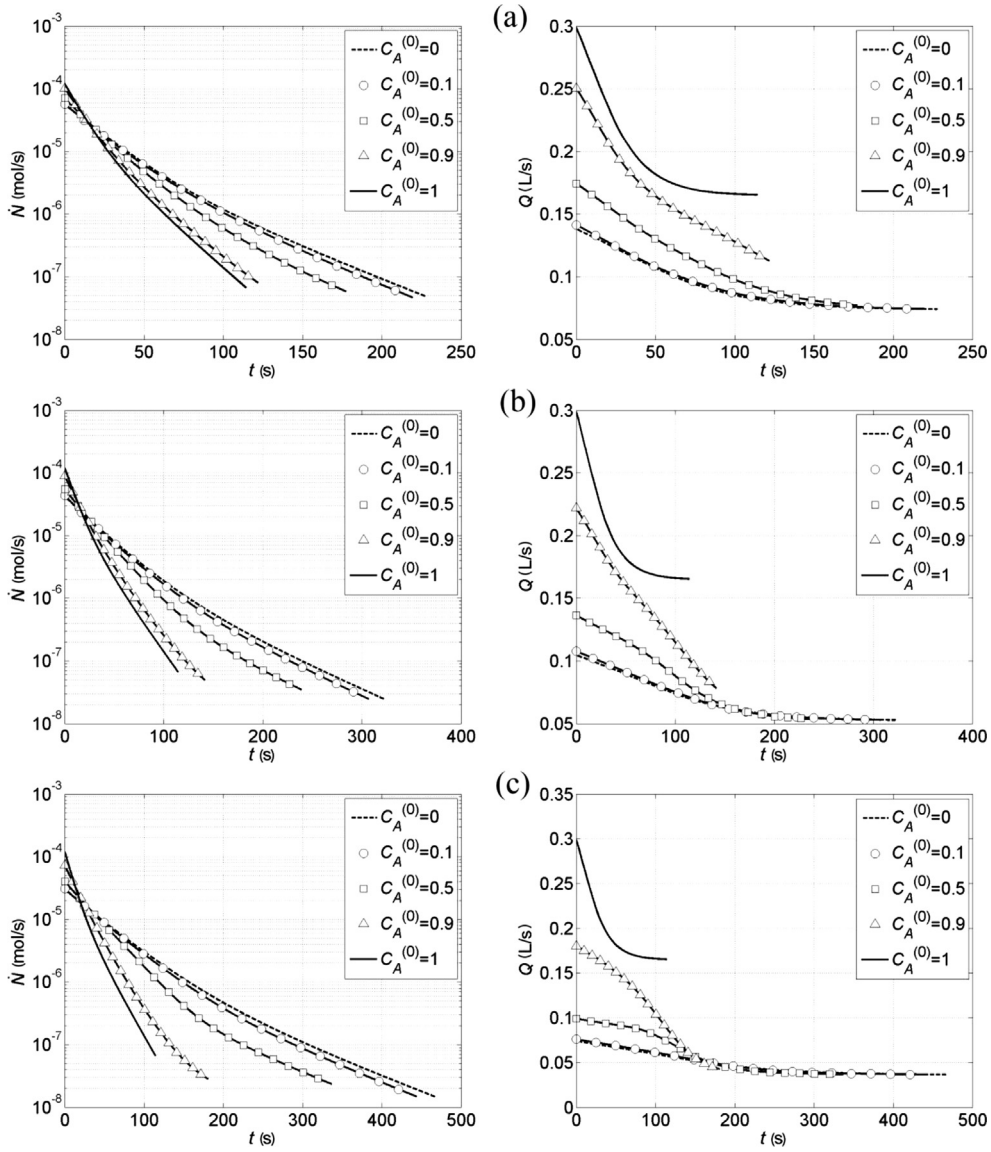

Fig. 6. Computational temporal evolution of the molar flow rate $\dot{N}(t)$ and conductance $Q(t)$ for the binary gas mixtures of (a) He–Ne, (b) He–Ar and (c) He–Kr with various initial molar fractions $C_A^{(0)}$.

In the present simulation, the flow initially is in the viscous regime ($P_A^{(0)} = 1000$ Pa) and at the end is in the free molecular regime ($P_A = 1$ Pa) and therefore it is expected that

$$1 \le Z = \frac{J_1}{J_2}\frac{1 - C_A}{C_A} \le \sqrt{\frac{m_2}{m_1}}. \tag{18}$$

In Fig. 8, the quantity Z is plotted versus time for the three binary gas mixtures under investigation, with $C_A^{(0)} = [0.1, 0.5, 0.9]$ in each mixture. In all cases the qualitative behaviour is similar. At $t = 0$, the value of Z is unity since the initial Knudsen numbers $Kn_A^{(0)}$ are always less than 0.04 (see Table 2) and no gas separation is taken place. Then, Z increases with time, and at the end of the process it approaches asymptotically the upper limiting value of $\sqrt{m_2/m_1}$, which for the binary gas mixtures of He–Ne, He–Ar and He–Kr is 2.24, 3.15 and 4.57 respectively (marked with the dotted lines in Fig. 8). It is also seen that Z increases slowly in the beginning and at the end of the process, when the flow is in the viscous and free molecular regimes respectively and rapidly in the intermediate times, when the flow is in the transition regime. It is evident that dZ/dt, i.e., the rate with which gas separation is increased, becomes maximum in the transition regime. In all mixtures the variation of Z with respect to time lasts longer as the molar fraction $C_A^{(0)}$ is decreased, i.e., as the amount of the light species is decreased.

5.3. The equivalent single gas approach

In several occasions in order to reduce modelling effort the so-called "equivalent single gas" approach is introduced. In this formulation the binary gas mixture is replaced by a single gas with effective molar mass $m^{(eq)} = Cm_1 + (1 - C)m_2$, where C is the molar fraction of the mixture and m_1, m_2 are the molar masses of the two components of the mixture. Thus, it is assumed that there is no separation effect and the analysis is identical to that of the single gas. In the present section, we assume that $C = C_A^{(0)}$ and $m^{(eq)} = m_A^{(0)}$. They are both taken to remain constant in the flow process. Based on this equivalent gas approach, the evolution of the gas pressure P_A in the chamber A and of the tube conductance Q is simulated and results are presented in Figs. 9 and 10 respectively for all three mixtures with $C = C_A^{(0)} = [0, 0.1, 0.5, 0.9, 1]$.

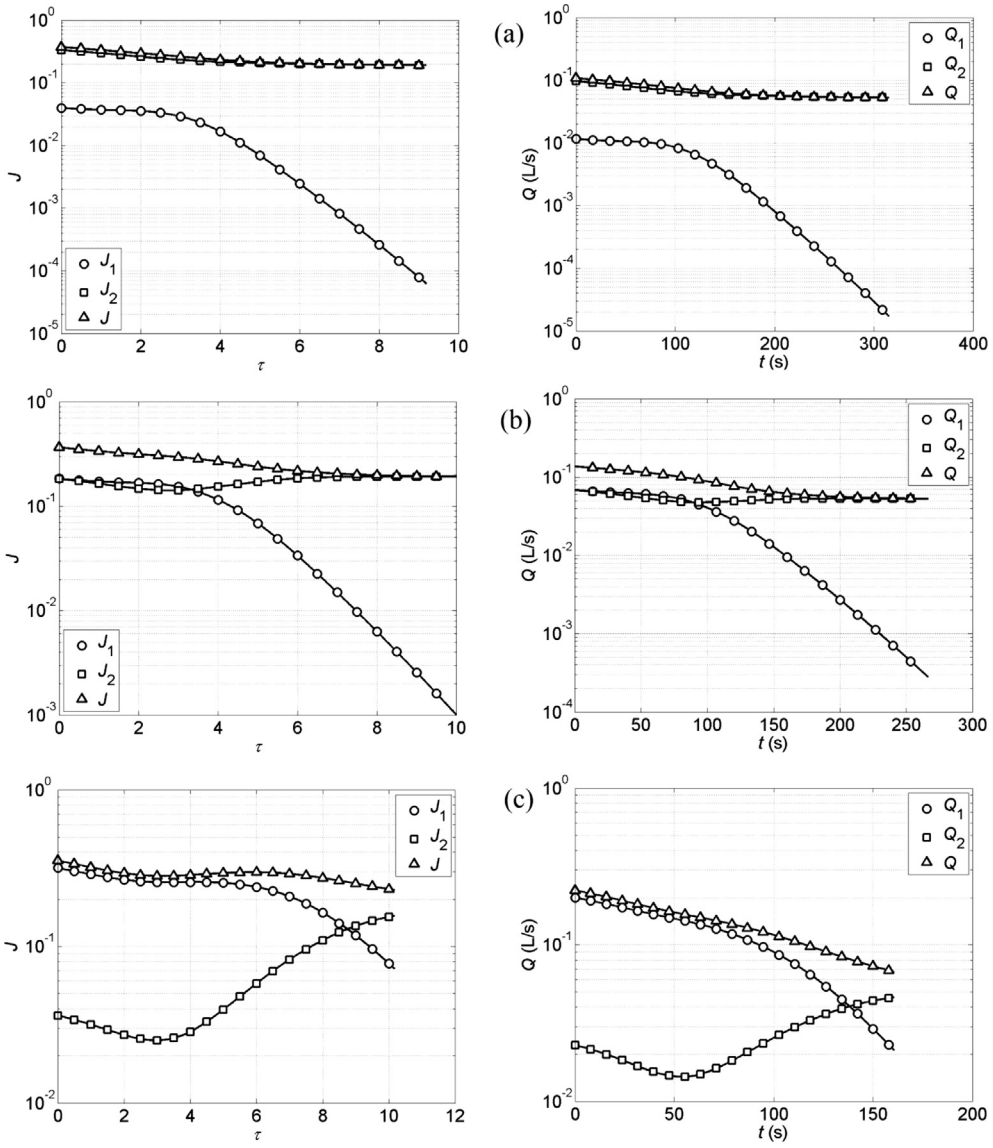

Fig. 7. Computational temporal evolution of dimensionless flow rates J_1, J_2 and conductance Q_1, Q_2 along with the corresponding total quantities $J = J_1 + J_2$, $Q = Q_1 + Q_2$ of the binary gas mixture of He–Ar for (a) $C_A^{(0)} = 0.1$, (b) $C_A^{(0)} = 0.5$ and (c) $C_A^{(0)} = 0.9$.

In Fig. 9, the pressure evolution $P_A(t)$ from 1000 Pa to 1 Pa for the equivalent gases is presented. The corresponding results based on the binary gas mixture analysis are also presented for comparison purposes. They are the same with the ones in Fig. 4 but now they are extended to a longer expansion time until the pressure reaches 1 Pa. Comparing the corresponding pressure evolutions between the equivalent single gas approach with the complete binary gas analysis, it is seen that the agreement is good in the case of He–Ne but deteriorates for He–Ar and the largest differences occur for He–Kr. In general, the differences are increased as the molar mass ratio m_2/m_1 of the components of the mixture is increased. Also, in all mixtures the agreement is worst for $C_A^{(0)} = 0.9$, it is improved for $C_A^{(0)} = 0.5$ and becomes quite good for $C_A^{(0)} = 0.1$. This is well explained, since separation is reduced as the molar fraction of the light gas is decreased.

These remarks are also supported by the corresponding tube conductance evolution $Q(t)$ plotted in Fig. 10. In the He–Ne mixture the equivalent single gas conductance is in good agreement with that of the binary gas mixture for a long time of the expansion process. This agreement is not as good for He–Ar and even worse for He–Kr, with the worst case being for He–Kr with $C_A^{(0)} = 0.9$. In general, the disagreement between corresponding results is increased as the expansion process evolves in time. This happens since, with the equivalent single gas approach, the variation of $C_A(t)$ in time due to gas separation cannot be taken into account. However in the cases of He–Ne and He–Ar and even for He–Kr with small $C_A^{(0)}$, the equivalent single gas approach provides reasonable good results within about ±20% for the overall quantities and it may be implemented, provided that the species quantities and separation effects are not important for the specific application.

6. Concluding remarks

The time-dependent flow of the single gases of He, Ne, Ar and Kr, as well as of the binary gas mixtures of He–Ne, He–Ar and He–Kr with various molar fractions from a chamber through a short tube into vacuum have been computationally investigated. The numerical solution is based on a simple explicit-type hybrid scheme,

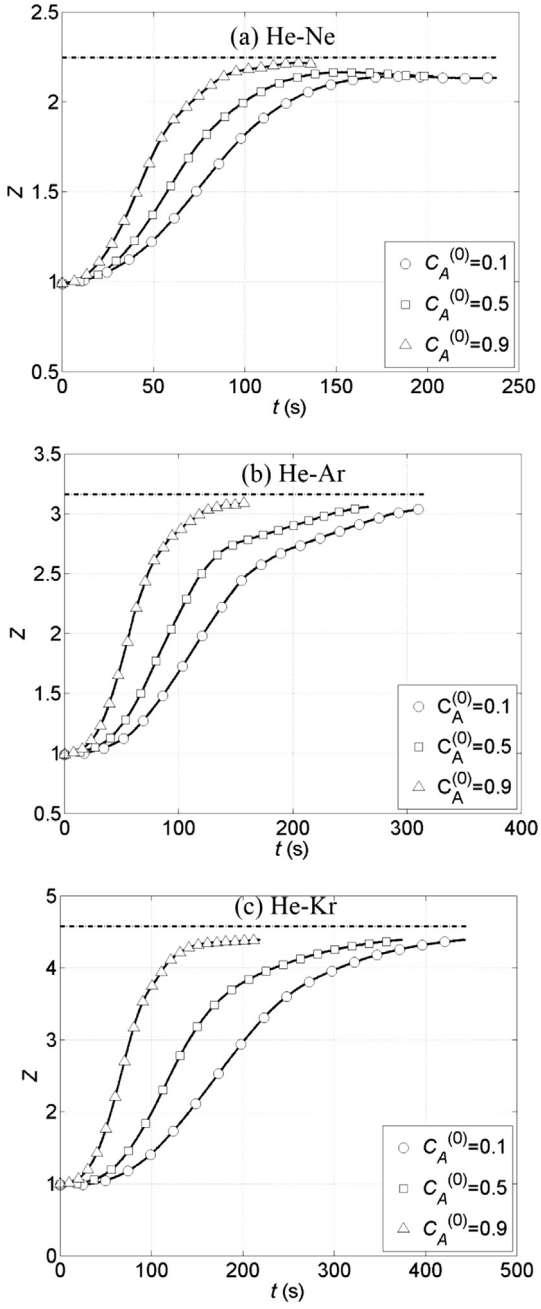

Fig. 8. Computational temporal evolution of $Z = (J_1/J_2)[(1 - C_A)/C_A]$ for the binary gas mixtures of (a) He–Ne, (b) He–Ar and (c) He–Kr with various initial molar fractions $C_A^{(0)}$.

where at each time step the tube flow rate is obtained through interpolation from a dense accordingly pre-constructed DSMC database (micro model) and then, the gas pressure and density in the chamber are updated by applying mass conservation (macro model). Experimental work is also performed in the PTB dynamic gas expansion facility by measuring the temporal pressure evolution in the chamber for all involved single cases and binary gas mixtures. By a comparison between corresponding computational and experimental results the applicability of the implemented hybrid modelling approach is demonstrated, where the observed difference of about 10% between the computed and experimental flow rates at each time step is mainly attributed to the measurement uncertainties of the tube and the vessel volume dimensions along with the resulting error accumulation for the pressure. In the case of binary gas mixtures, in addition to the total quantities, the temporal evolution of the molar flow rates and of the conductance of each species through the tube were also computed. The dependency of the binary gas mixture flow characteristics on the type of the components of the mixture as well as on its molar fraction has been examined and some insight in the separation phenomenon is provided. Also the differences and similarities between pure gases and binary mixtures are identified.

It has been found that as the mean molar mass of the binary mixture becomes smaller, the tube conductance is monotonically increased and the expansion process evolves faster. The binary gas mixture pressure evolution curves are always bounded by the

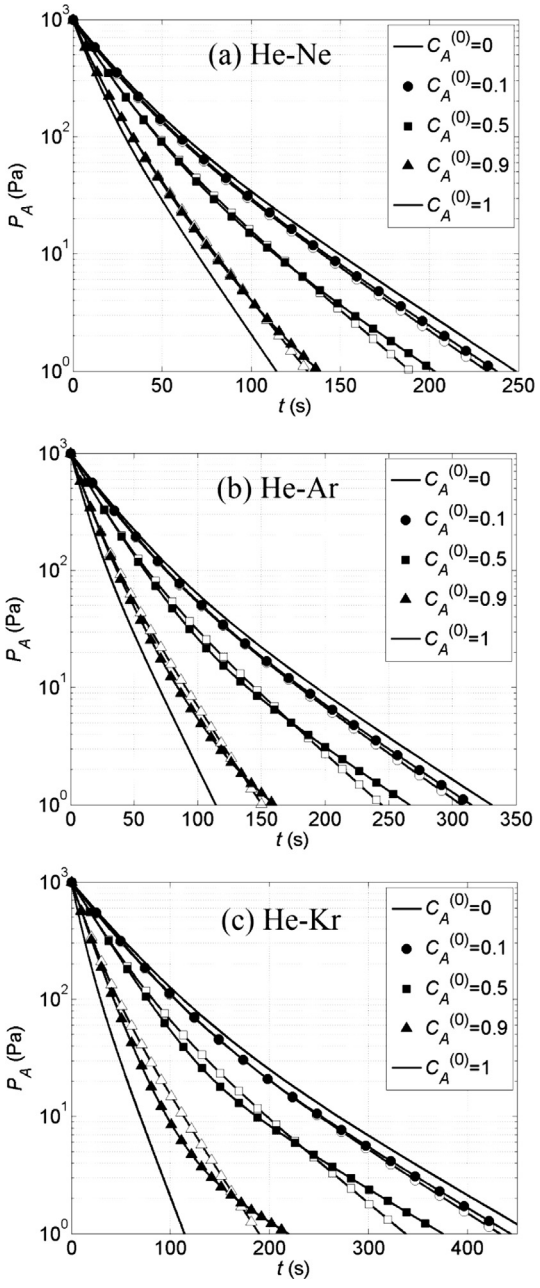

Fig. 9. Comparison between the computed temporal evolution of pressure P_A of the binary gas mixtures of He–Ne, He–Ar and He–Kr and various initial molar fractions $C_A^{(0)}$ (filled symbols) with the corresponding ones of the equivalent single gases (empty symbols).

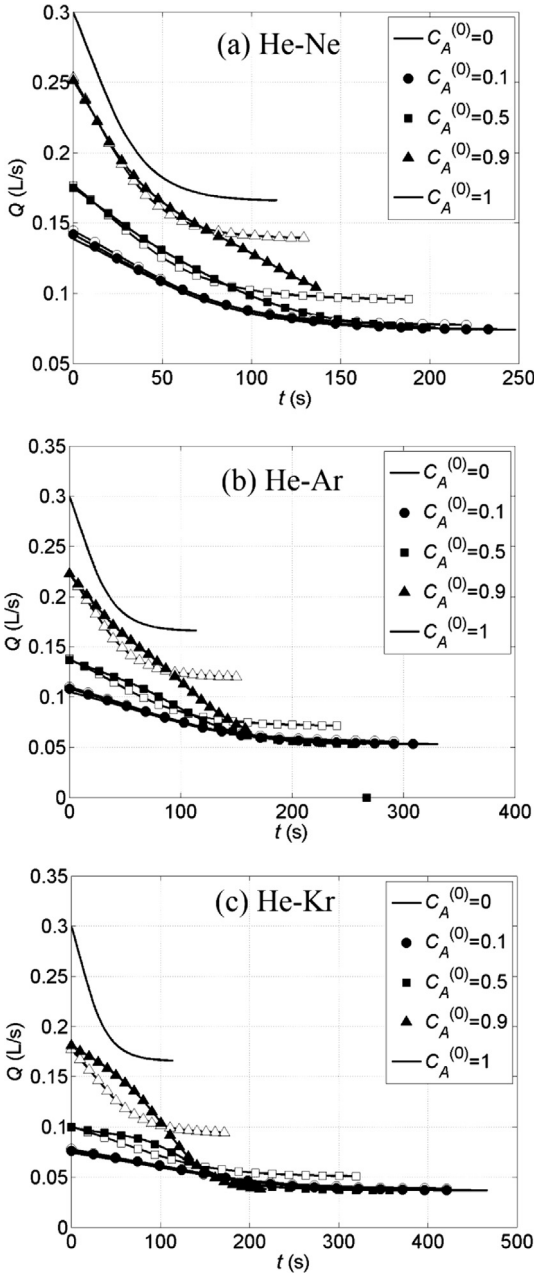

Fig. 10. Comparison between the computed temporal evolution of conductance Q of the binary gas mixtures of He–Ne, He–Ar and He–Kr and various initial molar fractions $C_A^{(0)}$ (filled symbols) with the corresponding ones of the equivalent single gases (empty symbols).

corresponding ones of the two components of the mixture flowing as single gases and more precisely from the light gas curve from below and the heavy gas curve from above, while it is the other way around for the conductance of the gas mixture through the tube. Investigating the temporal evolution of the species flow rates elucidates the gas separation phenomenon. Gas separation is monotonically increased as we move from the viscous towards the free molecular regime, while the rate with which gas separation is increased has a maximum in the transition regime. Furthermore the equivalent single gas approach, commonly used to reduce computational effort, has been examined and it has been found that in certain cases it may provide reasonably good results for the overall quantities.

Acknowledgements

Support through the EMRP IND12 project is gratefully acknowledged. The EMRP is jointly funded by the EMRP participating countries within EURAMET and the European Union. The authors would like to thank J. Buthig for his assistance in the experimental work.

Appendix. Micro model simulations based on the DSMC method

As described in Section 3, the steady-state single gas and binary gas mixture flow rates are obtained via a DSMC solver for HS molecules and purely diffuse reflection at the walls [14]. The species properties are taken from Table 2.

The computational domain consists of the tube with radius R and length L plus the inlet and outlet cylindrical volumes adjacent to the tube ends, defined by (R_1, L_1) and (R_2, L_2) respectively. These two volumes are taken large enough ($R_1 = R_2 = L_1 = L_2 = 8R$) to ensure uniform conditions at the boundaries but still much smaller than the actual volumes of chambers A and B. A three-level axisymmetric computational grid is employed in order to capture the gradients close to the boundaries and weighting factors in the axial and radial direction are used to ensure a more uniform number of particles in cells. The cell size of the coarsest grid is $R/40$, which for the present tube with aspect ratio $L/R = 1$ results to a total number of 232,800 grid cells. The time step is chosen to be $\Delta t_m = 0.005R/v_A^{(0)}$ and the total number of particles is 25×10^6. The sampling starts once the steady state flow has been achieved and continues by time averaging until the relative scattering satisfies the termination condition $\sqrt{N^+}/(N^+ - N^-) < 0.003$, where N^+ and N^- denote the particles crossing the inlet cross section of the tube from left to right and from right to left respectively. The numerical uncertainty in the flow rates is less than 1%. All simulations have been performed in dimensionless form.

The kinetic database of J_1 and J_2 in terms of the upstream rarefaction parameter, defined as $\delta_A = \sqrt{\pi}/(2Kn_A)$, and the molar fraction C_A are presented in Table 3. Results are provided for all three mixtures included in the investigation for $\delta_A = 0$, 0.1, 0.5, 1, 5, 10, 50, 100 and $C_A = 0$, 0.125, 0.25, 0.375, 0.5, 0.675, 0.750, 0.875, 1. The values of J_1 and J_2 for $C_A = 0$ and 1 correspond to the flow rates of the single gas and as expected they coincide. The values of this database, which is adequately dense to provide accurate results, are introduced accordingly at each time step of the hybrid scheme and whenever needed time interpolation between the available data is performed. The results are provided, on purpose, in tabulated form in order to be easily accessible in the present and future works.

Table 3
Database of steady-state flow rates of three binary gas mixtures for various values of the molar fraction $C_A^{(0)} \in [0, 1]$ and the gas rarefaction parameter $\delta_A^{(0)} \in [0, 100]$.

$C_A^{(0)}$	$\delta_A^{(0)}$	He–Ne		He–Ar		He–Kr	
		J_1	J_2	J_1	J_2	J_1	J_2
0	0	0	0.190	0	0.190	0	0.190
	0.1	0	0.192	0	0.192	0	0.192
	0.5	0	0.202	0	0.202	0	0.202
	1	0	0.213	0	0.213	0	0.213
	5	0	0.267	0	0.267	0	0.267
	10	0	0.300	0	0.300	0	0.300
	50	0	0.363	0	0.363	0	0.363
	100	0	0.383	0	0.383	0	0.383

(*continued on next page*)

Table 3 (*continued*)

$C_A^{(0)}$	$\delta_A^{(0)}$	He–Ne		He–Ar		He–Kr	
		J_1	J_2	J_1	J_2	J_1	J_2
0.125	0	0.0505	0.157	0.0708	0.156	0.102	0.156
	0.1	0.0499	0.160	0.0700	0.159	0.100	0.158
	0.5	0.0488	0.170	0.0669	0.169	0.0955	0.168
	1	0.0468	0.181	0.0638	0.179	0.0896	0.179
	5	0.0401	0.234	0.0488	0.234	0.0620	0.235
	10	0.0401	0.263	0.0440	0.264	0.0509	0.265
	50	0.0451	0.320	0.0454	0.320	0.0454	0.320
	100	0.0485	0.338	0.0485	0.338	0.0482	0.338
0.25	0	0.0951	0.127	0.131	0.125	0.190	0.124
	0.1	0.0948	0.130	0.131	0.128	0.187	0.127
	0.5	0.0925	0.139	0.126	0.137	0.180	0.136
	1	0.0900	0.150	0.120	0.148	0.169	0.147
	5	0.0798	0.201	0.0948	0.201	0.120	0.201
	10	0.0801	0.227	0.0874	0.229	0.101	0.230
	50	0.0911	0.275	0.0917	0.275	0.0921	0.276
	100	0.0965	0.290	0.0968	0.290	0.0967	0.289
0.375	0	0.134	0.0993	0.183	0.0965	0.260	0.0952
	0.1	0.133	0.101	0.182	0.0987	0.258	0.0976
	0.5	0.131	0.110	0.176	0.107	0.249	0.106
	1	0.129	0.120	0.170	0.117	0.236	0.117
	5	0.118	0.167	0.139	0.168	0.173	0.169
	10	0.120	0.190	0.130	0.192	0.150	0.194
	50	0.137	0.230	0.137	0.231	0.139	0.232
	100	0.145	0.242	0.143	0.242	0.143	0.242
0.5	0	0.165	0.0733	0.222	0.0702	0.313	0.0686
	0.1	0.165	0.0753	0.221	0.0725	0.311	0.0707
	0.5	0.164	0.0827	0.216	0.0801	0.302	0.0787
	1	0.162	0.0911	0.210	0.0891	0.290	0.0880
	5	0.155	0.133	0.179	0.135	0.221	0.136
	10	0.159	0.153	0.172	0.155	0.194	0.158
	50	0.182	0.184	0.183	0.185	0.185	0.187
	100	0.191	0.195	0.192	0.194	0.192	0.194
0.625	0	0.188	0.0502	0.248	0.0471	0.345	0.0451
	0.1	0.189	0.0516	0.247	0.0485	0.343	0.0468
	0.5	0.190	0.0575	0.244	0.0550	0.336	0.0534
	1	0.190	0.0646	0.240	0.0626	0.325	0.0612
	5	0.191	0.0990	0.216	0.101	0.262	0.102
	10	0.198	0.115	0.212	0.118	0.239	0.120
	50	0.229	0.138	0.229	0.139	0.234	0.140
	100	0.239	0.146	0.239	0.146	0.240	0.146
0.75	0	0.201	0.0299	0.256	0.0269	0.348	0.0251
	0.1	0.203	0.0307	0.256	0.0281	0.347	0.0266
	0.5	0.206	0.0350	0.257	0.0327	0.344	0.0312
	1	0.210	0.0398	0.256	0.0384	0.338	0.0371
	5	0.223	0.0652	0.247	0.0669	0.294	0.0682
	10	0.236	0.0762	0.250	0.0784	0.278	0.0810
	50	0.272	0.0931	0.276	0.0928	0.281	0.0937
	100	0.287	0.0979	0.287	0.0976	0.289	0.0975
0.875	0	0.203	0.0129	0.242	0.0109	0.310	0.0097
	0.1	0.205	0.0135	0.243	0.0115	0.311	0.0103
	0.5	0.212	0.0155	0.248	0.0140	0.314	0.0128
	1	0.219	0.0181	0.252	0.0170	0.315	0.0160
	5	0.250	0.0316	0.269	0.0327	0.309	0.0334
	10	0.272	0.0378	0.283	0.0386	0.308	0.0403
	50	0.319	0.0465	0.321	0.0465	0.327	0.0470
	100	0.335	0.0496	0.336	0.0488	0.337	0.0490
1	0	0.190	0	0.190	0	0.190	0
	0.1	0.192	0	0.192	0	0.192	0
	0.5	0.202	0	0.202	0	0.202	0
	1	0.213	0	0.213	0	0.213	0
	5	0.267	0	0.267	0	0.267	0
	10	0.300	0	0.300	0	0.300	0
	50	0.363	0	0.363	0	0.363	0
	100	0.383	0	0.383	0	0.383	0

References

[1] Lihnaropoulos J, Valougeorgis D. Unsteady vacuum gas flow in cylindrical tubes. Fusion Eng Des 2011;86:2139–42.
[2] Sharipov F. Transient flow of rarefied gas through an orifice. J Vac Sci Technol A 2012;30(2):021602.
[3] Sharipov F. Transient flow of rarefied gas through a short tube. Vacuum 2013;90:25–30.
[4] Jousten K, Pantazis S, Buthig J, Model R, Wuest M, Iwicki J. A standard to test the dynamics of vacuum gauges in the millisecond range. Vacuum 2014;100:14–7.
[5] Sonderegger K, Dur M, Buthig J, Pantazis S, Jousten K. Very fast-opening UHV gate valve. J Vac Sci Technol A 2013;31:060601.
[6] Sharipov F, Graur I. General approach to transient flows of rarefied gases through long capillaries. Vacuum 2014;100:14–7.
[7] Vargas M, Naris S, Valougeorgis D, Pantazis S, Jousten K. Hybrid modeling of time-dependent rarefied gas expansion. J Vac Sci Technol A 2014;32(2):021602.
[8] Lockerby DA, Duque-Daza CA, Borg MK, Reese JM. Time-step coupling for hybrid simulations of multi-scale flows. J Comput Phys 2013;237:344–65.
[9] Lafferty JM. Foundations of vacuum science and technology. New York: John Wiley & Sons Inc.; 1998.
[10] Ota M, He Y, Stefanov SK. 25th rarefied gas dynamics. In: Rebrov AK, Ivanov MS, editors. AIP conference proceedings, Novosibirsk; 2007. p. 1134.
[11] He Y, Stefanov SK, Ota M. 26th rarefied gas dynamics. In: Abe T, editor. AIP conference proceedings, 1084; 2008. p. 281.
[12] Sharipov F. Gaseous mixtures in vacuum systems and microfluidics. J Vac Sci Technol A 2013;31(5):050806.
[13] Bird GA. Molecular gas dynamics and the direct simulation of gas flows. Oxford: Oxford University Press; 1994.
[14] Stefanov SK. On DSMC calculations of rarefied gas flows with small number of particles in cells. SIAM J Sci Comput 2011;33(2):677–702.
[15] Aristov VV. Direct methods for solving the Boltzmann equation and study of non-equilibrium flows. Dordrecht: Kluwer Academic Publishers; 2001.
[16] Titarev VA. Rarefied gas flow in a circular pipe of finite length. Vacuum 2013;94:92–103.
[17] Pantazis S, Valougeorgis D. Rarefied gas flow through a cylindrical tube due to a small pressure difference. Eur J Mech B Fluids 2013;38:114–27.
[18] Aristov VV, Shakhov EM, Titarev VA, Zabelok SA. Comparative study for rarefied gas flow into vacuum through a short circular pipe. Vacuum 2014;103:5–8.
[19] Sharipov F. Numerical simulation of rarefied gas flow through a thin orifice. J Fluid Mech 2004;518:35–60.
[20] Lilly TC, Gimelshein SF, Ketsdever AD, Markelov GN. Measurements and computations of mass flow and momentum flux through short tubes in rarefied gases. Phys Fluids 2006;18:093601.
[21] Varoutis S, Sazhin O, Valougeorgis D, Sharipov F. Rarefied gas flow through short tubes into vacuum. J Vac Sci Technol A 2008;26(2):228–38.
[22] Varoutis S, Valougeorgis D, Sharipov F. Gas flow through tubes of finite length over the whole range of rarefaction for various pressure drop ratios. J Vac Sci Technol A 2009;27(6):1377–91.
[23] Sazhin O. Impact of the gas-surface scattering and gas molecule-molecule interaction on the mass flow rate of the rarefied gas through a short channel into a vacuum. J Vac Sci Technol A 2010;28(6):1393–8.
[24] Szalmas L, Valougeorgis D, Colin S. DSMC simulation of pressure driven binary rarefied gas flows through short microtubes. In: ASME – 9th international conference on nanochannels, microchannels, and minichannels, paper ICNMM11-58022, Edmonton, Canada; 2011.
[25] Pantazis S, Rusche H. A hybrid continuum-particle solver for unsteady rarefied gas flows. Vacuum 2014;109:275–83.
[26] Pantazis S, Jousten K. Computational and experimental study of unsteady gas flow in a dynamic vacuum standard. Vacuum 2014;109:373–84.
[27] Titarev VA, Shakhov EM. Computational study of a rarefied gas flow through a long circular pipe into vacuum. Vacuum 2012;86:1709–16.
[28] Sharipov F. Benchmark problems in rarefied gas dynamics. Vacuum 2012;86:1697–700.
[29] Marino L. Experiments on rarefied gas flows through tubes. Microfluid Nanofluidics 2009;6(1):109–19.
[30] Sharipov F, Strapasson JL. Ab initio simulation of rarefied gas flow through a thin orifice. Vacuum 2014;109:246–52.
[31] Varoutis S, Naris S, Hauer V, Day C, Valougeorgis D. Experimental and computational investigation of gas flows through long channels of various cross sections in the whole range of the Knudsen number. J Vac Sci Technol A 2009;27(1):89–100.